Published in "Interface Focus 7(4): 20160129, 2017
which should be cited to refer to this work.

Circularly polarized reflection from the scarab beetle *Chalcothea smaragdina*: light scattering by a dual photonic structure

Luke T. McDonald[1,2], Ewan D. Finlayson[1], Bodo D. Wilts[3] and Pete Vukusic[1]

[1]Department of Physics and Astronomy, University of Exeter, Stocker Road, Exeter EX4 4QL, UK
[2]School of Biological, Earth and Environmental Sciences, University College Cork, North Mall Campus, Cork, Republic of Ireland
[3]Adolphe Merkle Institute, University of Fribourg, Chemin des Verdiers 4, 1700 Fribourg, Switzerland

Helicoidal architectures comprising various polysaccharides, such as chitin and cellulose, have been reported in biological systems. In some cases, these architectures exhibit stunning optical properties analogous to ordered cholesteric liquid crystal phases. In this work, we characterize the circularly polarized reflectance and optical scattering from the cuticle of the beetle *Chalcothea smaragdina* (Coleoptera: Scarabaeidae: Cetoniinae) using optical experiments, simulations and structural analysis. The selective reflection of left-handed circularly polarized light is attributed to a Bouligand-type helicoidal morphology within the beetle's exocuticle. Using electron microscopy to inform electromagnetic simulations of this anisotropic stratified medium, the inextricable connection between the colour appearance of *C. smaragdina* and the periodicity of its helicoidal rotation is shown. A close agreement between the model and the measured reflectance spectra is obtained. In addition, the elytral surface of *C. smaragdina* possesses a blazed diffraction grating-like surface structure, which affects the diffuse appearance of the beetle's reflected colour, and therefore potentially enhances crypsis among the dense foliage of its rainforest habitat.

1. Background

Benefiting from millions of years of evolution, complex growth and formation mechanisms are used by numerous biological systems [1–5], often producing remarkable optical effects [6–8]. Animals, plants and minerals showcase an extraordinary diversity of biological photonic blueprints, illuminating the path towards designing dynamic and adaptive photonic devices [9–11]. The order Coleoptera is no exception [12], comprising approximately 400 000 species, many of which display interesting optical properties including: narrowband and broadband metallic colours [13,14], iridescent appearances [15–17], brilliant whiteness [18,19] and distinct polarization signatures [20–22].

Polarized light is exploited extensively throughout nature. Particularly in the animal kingdom, polarized light assists in predation [23,24], navigation [25,26] and intraspecific communication [27,28] within a variety of ecosystems. In contrast to linear polarization effects, which have been reported in numerous biological systems [29–32], encountering circular polarization (CP) in nature is, broadly speaking, far less common. The reflection of elliptically polarized light, with a high degree of CP (ellipticity close to ± 1), is limited to a narrow range of organisms, primarily arthropods, with the highest concentration of species exhibiting CP structural colours belonging to the coleopteran family Scarabaeidae. Among scarabaeid beetles, Michelson is attributed with the earliest observation of this phenomenon, described in his 1911 study 'On metallic colouring in birds and insects' [33]. Early follow-up work showed that the optical properties of

certain scarabaeids were analogous to those exhibited by ordered cholesteric liquid crystal phases [34,35]. The advent of electron microscopy facilitated significant advancements in the understanding of the similarities in structural organization shared by liquid crystals and biological materials. Consequently, several investigations uncovered the precise physical origin of the optical activity displayed by these systems shed new light on the beetles' photonic ultrastructure [21,36–39].

In beetle species reflecting CP light, an ultrastructure comprising clusters of parallel aligned chitin microfibrils woven into a lamellar architecture within the exocuticle was described. Upon transitioning adjacent microfibril planes, the microfibrils are rotated by small angles, for example, around 7–8° [40], thereby creating a helicoidal morphology. The rotation of this assembly through an angle of 180° forms the eponymous 'Bouligand structure' [21,39] typically associated with the exocuticle structures of many arthropods [41], including decapods [42–44] and stomatopods [45,46] in addition to scarabaeid beetle species. Beyond the animal kingdom, helicoidal morphologies assembled from cellulose have been reported in fruits [47,48] and other plants [49,50].

Overwhelmingly, investigations into the reflection of CP light by scarabaeid beetles show that they exclusively reflect left-handed CP (LCP) light in response to illumination at normal incidence [22,51,52]. Presently, the 'jewel scarab' *Chrysina resplendens*, coincidently the subject of Michelson's initial observations [33], stands alone in exhibiting any deviation from this behaviour [53,54]; a modification to the exocuticle ultrastructure of *C. resplendens* enables this species to reflect both LCP and right-handed CP (RCP) light simultaneously. In this beetle, two spatially distinct left-handed helicoids are separated by a non-helicoidal layer that performs the function of a half-wave retarder; incident RCP light is reflected by the lower of these helicoids. Clockwise-rotating helicoidal structures that directly reflect RCP light are extremely rare, but are found alongside left-handed structures in the *Pollia condensata* fruit [47].

Known for their vibrant colours, beetles belonging to the Cetoniinae subfamily (flower chafers) present a plenitude of candidate specimens for optical characterization. Of particular relevance to this study, the reflection of CP light has been reported in several cetoniine species [52]. In this paper, we describe the CP colour appearance and light scattering properties of the flower chafer *Chalcothea smaragdina* through the use of a range of microscopy techniques, visible light spectroscopy, imaging scatterometry and theoretical modelling.

2. Material and methods

2.1. Beetle samples

Chalcothea smaragdina specimens were obtained from a commercial insect retailer (http://www.insect-sale.com). Cuticle samples were examined from numerous exoskeleton sites across multiple specimens; the micrographic and optical analyses presented herein concentrate on samples removed from the specimens' dorsal regions.

2.2. Optical imaging

Chalcothea smaragdina specimens were photographed with a Canon EOS-1000D camera equipped with a Canon EF 12 II extension tube. Each specimen was photographed through an LCP analyser, an RCP analyser (both Edmund Optics) and without any polarizer between the camera and the specimen. Small elytral samples, typically measuring 1–2 mm^2, were examined using a Zeiss Axiocam MRc5 USB camera connected to a Zeiss Axioskop 2 polarizing optical microscope. The *C. smaragdina* samples were imaged using both bright- and dark-field illumination, with CP analysers positioned in the illuminating and reflected light-paths. CP imaging was performed using custom-made Zeiss polarizers comprising a linear polarizer in conjunction with a quarter-wave retarder and also employed in the microspectrophotometry and imaging scatterometry set-ups.

2.3. Atomic force microscopy

The surface topology of the exterior exoskeleton was imaged using atomic force microscopy (AFM) for sample areas measuring $50 \times 50\,\mu m$. For this analysis, cuticle samples were cut and mounted on AFM stubs. Measurements were performed using a Nanosurf NaioAFM instrument, equipped with a Nanosensors PPP-EFM silicon cantilever, in dynamic mode.

2.4. Scanning electron microscopy

The ultrastructure of the surface of *C. smaragdina* was imaged using an FEI Nova 600 dual-beam field-emission scanning electron microscopy (SEM) with an electron beam voltage of 10 kV and a 7.5 pA beam current. Exoskeleton samples were glued to an SEM stub using electrically conducting epoxy resin and subsequently sputter coated with ≈ 6 nm of gold palladium.

2.5. Transmission electron microscopy

Samples were prepared for transmission electron microscopy (TEM) using a multi-stage process. The samples were first fixed in 3% glutaraldehyde at 21°C for 2 h, followed by rinsing in a sodium cacodylate buffer. Subsequent fixing in 1% osmic acid for 1 h preceded: dehydration through an ethanol series (ending with 100% ethanol), bathing in propylene oxide for 30 min and embedding in Spurr resin. After ultrathin-sectioning using an ultra-microtome, the samples were stained using first 2% uranyl acetate and, second, lead citrate before being examined using a JEOL 100S TEM instrument.

2.6. Circularly polarized reflectance spectrophotometry

Spectral reflectance measurements of the specimen's CP response were made using an Ocean Optics HPX-2000 broadband fibre-coupled light source (185–2000 nm) and an Ocean Optics USB2000+ spectrometer (200–850 nm). CP light was produced using a rotatable polarizer, followed by an achromatic Fresnel rhomb quarter-wave retarder, oriented at 45° azimuth. The Fresnel rhomb imposes a retardation of $\pi/2$ via two instances of total internal reflection. The CP handedness was selected by setting the polarizer azimuth to either 0° or 90°. Incident light was focused on to the sample, normal to its surface, using an achromatic 10X objective lens, producing a beam spot with a diameter of $\approx 30\,\mu m$. The reflected light was collected by the same lens before being subsequently directed through a CP analyser comprising the Fresnel rhomb and a second rotatable polarizer. The system was calibrated against a plane aluminium mirror of known reflectance.

2.7. Imaging scatterometry

The far-field spatial distribution of the light scattered from the beetles' elytra was visualized using an imaging scatterometer (ISM) [55]. The central component of the ISM is an ellipsoidal mirror. Small elytral samples are mounted to the tip of a micropipette and positioned in the mirror's first focal plane. Therefore, light scattered by the sample into the frontal hemisphere is focused by the mirror in its second focal plane and projected by a lens onto its back focal plane, thereby compressing the

far-field scattering pattern into an image that may be captured using a CCD camera. Two different illumination conditions are possible: (i) narrow-beam illumination through a central hole of the ellipsoidal mirror; (ii) wide-angle illumination via illumination through the ellipsoidal mirror by light focused from the second focal-point [56]. Custom-written MATLAB (http://www.mathworks.com) programs correct the resultant scatterograms for aberrations. A piece of MgO served as a white standard.

2.8. Optical modelling

By adopting the 4×4 matrix methodologies for one-dimensional anisotropic stratified media [57–59] and further incorporating the scattering matrix modification described by Ko & Sambles [60], a custom-written code compiled in MATLAB was used to model the CP reflectance arising due to the specimen's cuticle ultrastructure. The helicoidal pitch was assumed to vary continuously throughout the chiral exocuticle, with a resolution of 16 'sublayers' per helicoidal period, which was sufficient for the model to converge. The software package ImageJ (http://rsbweb.nih.gov/ij/) was used to analyse TEM cross-sections of the ultrastructure; lamellar pitch lengths, equivalent to eight 'sublayers', were extracted to create profiles of the helicoidal pitch fluctuation, which subsequently informed the 'sublayer' thicknesses applied in the modelling. A wavelength-dependent average for the real component of the refractive index (modelled using the Sellmeier relation, equation (3.1)) was used to describe the chitinous ultrastructure, with a fixed extinction coefficient and a fixed birefringence. Incoherent averaging was applied to account for localized variations in the lamellar pitch values fed into the model, which reduces spectral modulation [54].

3. Results

3.1. Optical appearance and spectral characteristics

The cetoniine scarab beetle *Chalcothea smaragdina* (Gory & Percheron 1833 [61]; Coleoptera: Scarabaeidae: Cetoniinae) is indigenous to Indonesia. The body of this flower chafer grows up to 3 cm in length, with all dorsal regions distinctly metallic green in appearance. Contrary to many other scarabaeid beetles, the body is elongated and features a pronounced, angular pronotum.

Figure 1*a–c* shows photographs of a beetle under different circular polarizers that provide a qualitative assessment of the specimen's CP properties. In common with the CP response typically associated with several genera of scarabaeid beetles [22,37,51,52], the photographs illustrate that *C. smaragdina* exhibits the selective reflection of LCP light exclusively. Observing *C. smaragdina* through an LCP analyser thus accentuates the specimen's metallic green colour appearance; by contrast, repeating the observation using an RCP analyser leads to the specimen's colour being effectively extinguished over the entirety of its exoskeleton.

Closer inspection of the exoskeleton surface using optical microscopy is shown in figure 1*d–g*. The images reveal the elytral surface to possess a reticulated structure comprising elongated, irregularly shaped domains that run approximately latitudinally across the whole breadth of the elytra. This morphology is most starkly represented in the optical micrograph corresponding to dark-field illumination (figure 1*e*), leading to the inference that this reticulated surface patterning dominates the beetle's colour at oblique angles; the domain interiors predominantly exhibit specular reflection. As shown

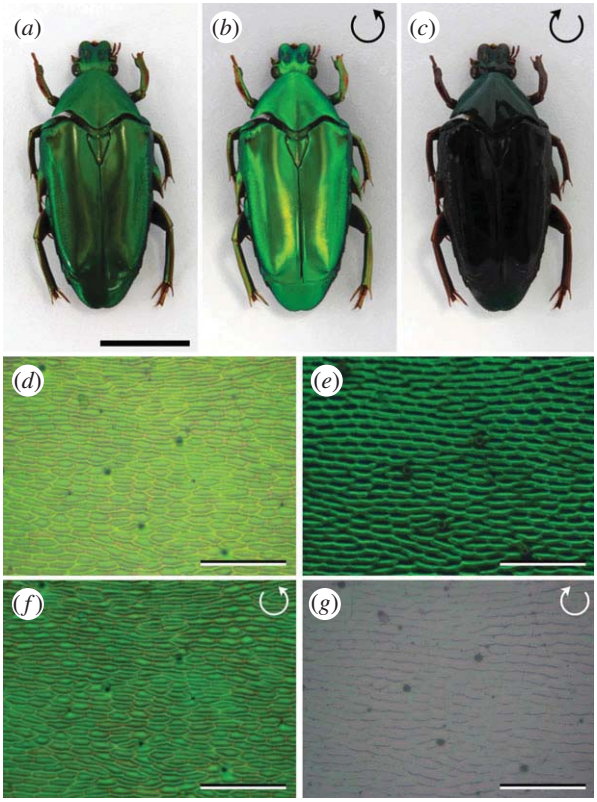

Figure 1. (*a–c*) Photographs of *C. smaragdina* capturing the beetle's appearance for the following configurations: (*a*) without an analysing filter, (*b*) through an LCP analyser and (*c*) through an RCP analyser. The photographs show that the beetle selectively reflects LCP light. (*d–g*) Optical micrographs of the elytral surface corresponding to: (*d*) unpolarized bright-field illumination; (*e*) unpolarized dark-field illumination; (*f*) with the reflected light analysed using an LCP filter; (*g*) with the reflected light analysed using an RCP filter. A reticulated surface patterning is revealed which scatters light to oblique angles under dark-field illumination. Scale bars, (*a*) 1 cm and (*d–g*) 50 μm.

in figure 1*b*,*c* respectively, the photographs using an LCP and RCP filter show the strong accentuation and depletion of the specimen's green colour appearance. To quantify this, we measured the CP-dependent reflectance of the elytral surface, shown in figure 2*a*. For LCP light, a pronounced optical bandgap is observed, with a principal reflection peak centred at ≈ 565 nm and a less intense feature at ≈ 585 nm, which extends the long-wavelength band-edge. These spectral features correspond to the saturated green-orange colour observed in figure 1*b*,*f*; the RCP analysis shows an absence of distinguishable spectral features. Outside of the optical bandgap observed for the LCP spectrum, the cross-polarized reflection shown in figure 1*b* exhibits a relatively featureless Fresnel-type reflection. Confined to the bandwidth of the LCP co-polarized reflection feature, a small spectral modulation is displayed in the cross-polarized response.

3.2. Integument ultrastructure

To further explore the reticulated surface morphology identified in the optical micrographs, elytral samples were examined using both SEM and AFM. Elucidating the exterior features using SEM imaging resolved the precise topography of the reticulated surface structure. Typically, the elongated domains observed in the optical micrographs were not fully enclosed, with the mesh-like appearance arising due to

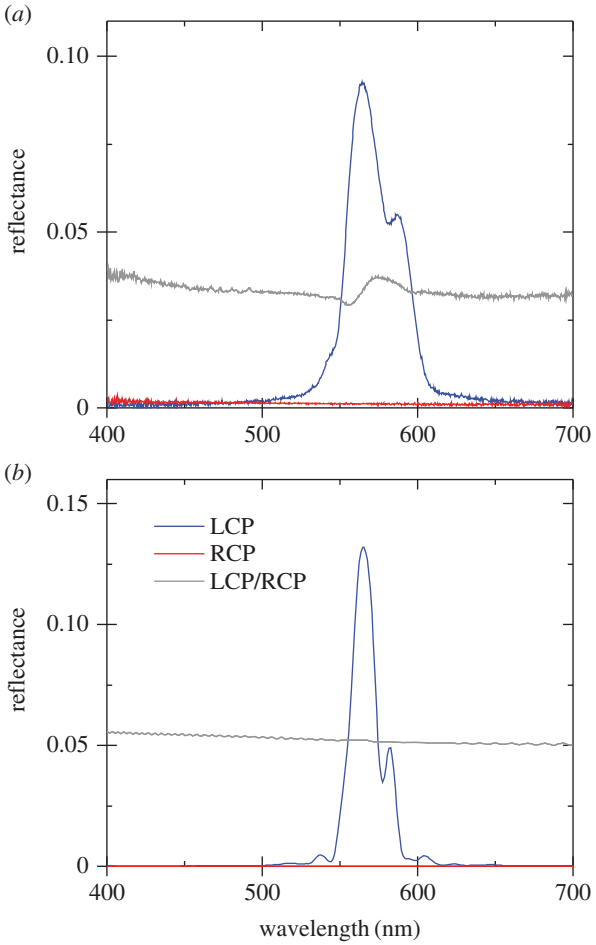

Figure 2. (*a*) Spectrophotometry measurements showing both the co-polarized (LCP and RCP) and cross-polarized (LCP/RCP) CP reflectance spectra for *C. smaragdina*. (*b*) Optical modelling of the co-polarized and cross-polarized reflectance from the specimen.

deviations in the direction followed by the otherwise approximately parallel surface striations (figure 3*a*). In addition, the edges of these striations were shown to possess a fine irregular sawtooth-like profile parallel to the surface plane (figure 3*b*). The surface topography was further explored using dynamic mode AFM to reveal a quasi-regular surface periodicity manifested by the pronounced acclivities and declivities at the edges of the striations (figure 3*c*). A line scan traversing the surface of *C. smaragdina* reveals that its surface topography closely resembles a blazed grating structure (figure 3*d*). Although the spacing between individual striations exhibits some variation due to the irregular geometry of the surface patterning, we found the grating structure to have a mean periodicity of 5.07 ± 0.11 µm. Analysis of AFM measurements from several elytral locations revealed that the blaze profile typically extends from the surface to a mean height of 118 ± 6 nm. These dimensions correspond to a blaze angle of $\approx 3.1^\circ$. The wavelength of light for which scattering is optimized by this configuration is $\lambda_b = 2a \sin\theta_b$, where a is the grating periodicity and θ_b is the blaze angle; substituting the values measured for *C. smaragdina* results in $\lambda_b \approx 548$ nm.

To determine the origin of the specimen's LCP colour appearance, the underlying photonic ultrastructure of *C. smaragdina* was investigated using TEM. The TEM cross-section image shown in figure 4*a* displays the exocuticle ultrastructure, responsible for producing the specimen's colour, in its entirety. A lamellar arrangement is apparent throughout the full depth of the exocuticle, which was measured to have a total thickness ranging from 10 to 11 µm across several sample locations. The inter-lamellar contrast is consistent with TEM studies of other CP reflectors identified in scarabaeid species [20,21,62], as opposed to the starkly contrasted alternating layers commonly observed in traditional coleopteran multilayer reflectors such as those found in buprestid beetles [32,63,64]. The lamellar appearance indicates that the *C. smaragdina* exocuticle comprises a helicoidal morphology (figure 4*c*), where the individual lamellae represent the rotation of the constituent chitin microfibrils through an angle of 180° and, therefore, the parallel alignment of the microfibrils. Thus, each lamellar pitch length corresponds to half the helicoidal period. This assembly is displayed clearly in the magnified TEM image shown in figure 4*b*. The inter-lamellar distances were measured to ascertain the distribution of lamellar pitch lengths throughout the depth of the exocuticle. The lamellar pitch profile for the *C. smaragdina* helicoid is presented in figure 4*d*. It shows that although the lamellar pitch length undulates continuously throughout the exocuticle, the amplitude of these undulations is small (≈ 5–10 nm). The profile shows that the lamellar pitch length varies between 160 and 180 nm, with the mean lamellar pitch length 169.7 ± 5.1 nm. Consequently, the mean pitch of the helicoid is ≈ 340 nm. Lamellar pitch profiles were constructed relating to several measurement locations from elytral samples, with the total number of lamellae measured showing high consistency, ranging from 68 to 72.

3.3. Modelling of the beetle's circular polarization reflectance

The analysis of the lamellar pitch distribution allowed us to perform electromagnetic simulations. For this, we implemented the ultrastructure of the exocuticle and calculated the total CP response at normal incidence, the results of which are presented in figure 2*b*. The helicoidal morphology comprising the exocuticle of *C. smaragdina* was treated as an anisotropic stratified medium with the helicoidal period defined using the TEM-based analysis outlined above. The calculated co-polarized and cross-polarized CP spectra shown in figure 2*b* correspond to an exocuticle structure comprising 35 full rotations of the helicoid. The specific sublayer thicknesses, from which the constituent helicoidal periods were constructed, were calculated using the mean lamellar pitch values represented by the green circles in figure 4*d*. As mentioned in §2.8, the average value of the real component of the structure's refractive index ($\bar{n}$) was described using the Sellmeier relation:

$$\bar{n}^2 = 1 + \frac{1.447776\lambda^2}{\lambda^2 - 0.017085}, \tag{3.1}$$

with the wavelength dimensions in micrometres. Subsequently, the real components of the extraordinary and ordinary refractive indices (n_e and n_o) were calculated using a fixed birefringence of $\Delta n = 0.018$ [53]. The basis for choosing these values is discussed further in §4.1. The modelled CP reflectance closely matches the experimental CP reflectance measurements shown in figure 2*a* with regards to the shape and position of the spectral features, particularly so for the co-polarized CP spectra. The small oscillatory feature recorded in the experimental measurement of the cross-polarized response, spanning the breadth of the LCP bandgap, was not replicated in the model. Additionally, the simulation predicts a slightly increased intensity in the LCP reflectance ($\approx 4\%$). The difference in intensity

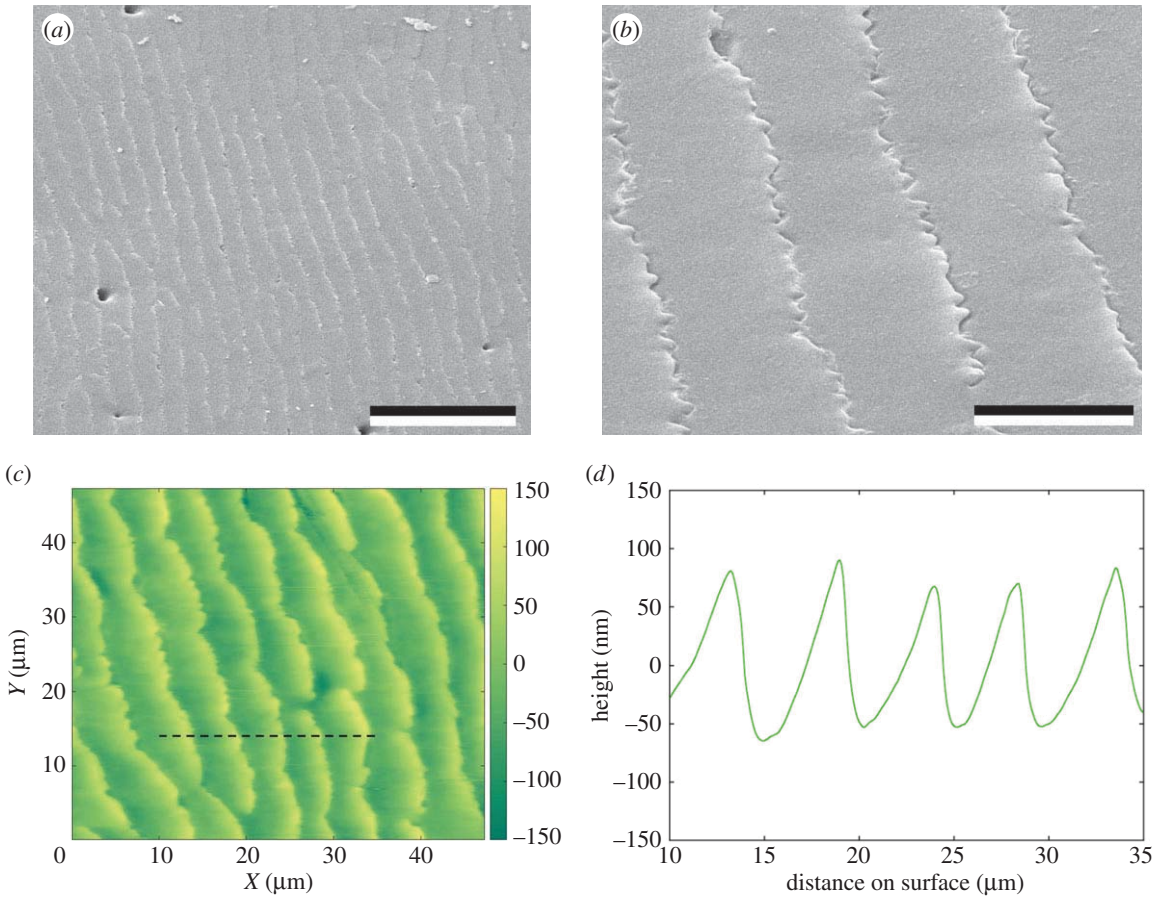

Figure 3. (*a*,*b*) SEM images detailing the reticulated elytral surface structure for *C. smaragdina*. (*c*,*d*) AFM measurements reveal the form of the blazed grating-like surface topography, with the dashed black line in (*c*) corresponding to the line profile shown in (*d*). Both techniques provided physical dimensions describing the blazed surface topography. Scale bars, (*a*) 30 μm and (*b*) 5 μm.

between the experimental and modelled LCP co-polarized response from the structure is discussed below.

3.4. Angle-dependency and scattering of circular polarization colour

The effect of both the blazed surface topography and the helicoidal ultrastructure on the reflection properties of *C. smaragdina* was further investigated using imaging scatterometry. Upon illumination of the elytron with an unpolarized, narrow-aperture light beam, the captured scattering pattern demonstrates highly directional reflection from the sample surface; a series of diffracted orders is observed, extending radially outwards from the image centre along the direction perpendicular to the surface striations (figure 5*a*). The green colour of the scattered light shows good agreement with the blaze wavelength anticipated from the analysis of the surface ultrastructure. We note that the central reflection, upon shorter exposure times, is also strongly green, in full accordance with the observations from optical microscopy (figure 1*d*,*f*).

When the sample is illuminated with a wide-aperture beam via the ellipsoidal mirror at the core of the scatterometer, the angle-dependency of the photonic structure in *C. smaragdina's* elytron can be assessed [32,56]. Figure 5*b* presents the scatterogram of the specimen's elytron using unpolarized light. The sample displays relatively weak iridescence, with the reflected green colour remaining essentially unaltered for scattering angles extending from normal incidence to approximately 50°. At this point, a slight blue-shift in the reflected hue is observed and an annulus of blue-green colour can be seen that extends to the circular line denoting a scattering angle of 60°. For larger scattering angles ($\gtrsim$60°), the surface reflectance becomes dominant and shows a strong whitish reflectance.

We repeated this measurement using an LCP and RCP analyser, respectively, positioned such that they acted to impart their CP handedness to the incident beam and also analyse the CP state of the reflected light. The LCP–LCP and RCP–RCP co-polarized scatterograms are shown in figure 5*c*,*d*, respectively. These scatterograms display close agreement with the optical images and CP reflectance spectra presented above. For scattering angles $\lesssim$60°, the specimen's LCP green reflected colour is more saturated compared to the unpolarized scatterogram (figure 5*b*), whilst the reflected colour is extinguished for the RCP-RCP scatterogram. The blue and brown fringes observed for scattering angles greater than 60° are artefacts that arise when investigating chiral samples using the ISM. Following oblique angle illumination with CP light, the handedness of the reflected light loses its purity at high scattering angles since the degree of CP is diminished. The coloured fringes correspond to the axes of the linear polarizer component of the analysing filter and are attributed to the chromatic dispersion of the analyser.

4. Discussion

4.1. Optical effect of the helicoidal morphology

In selectively reflecting LCP light, *C. smaragdina* displays the archetypal optical response associated with Bouligand-type

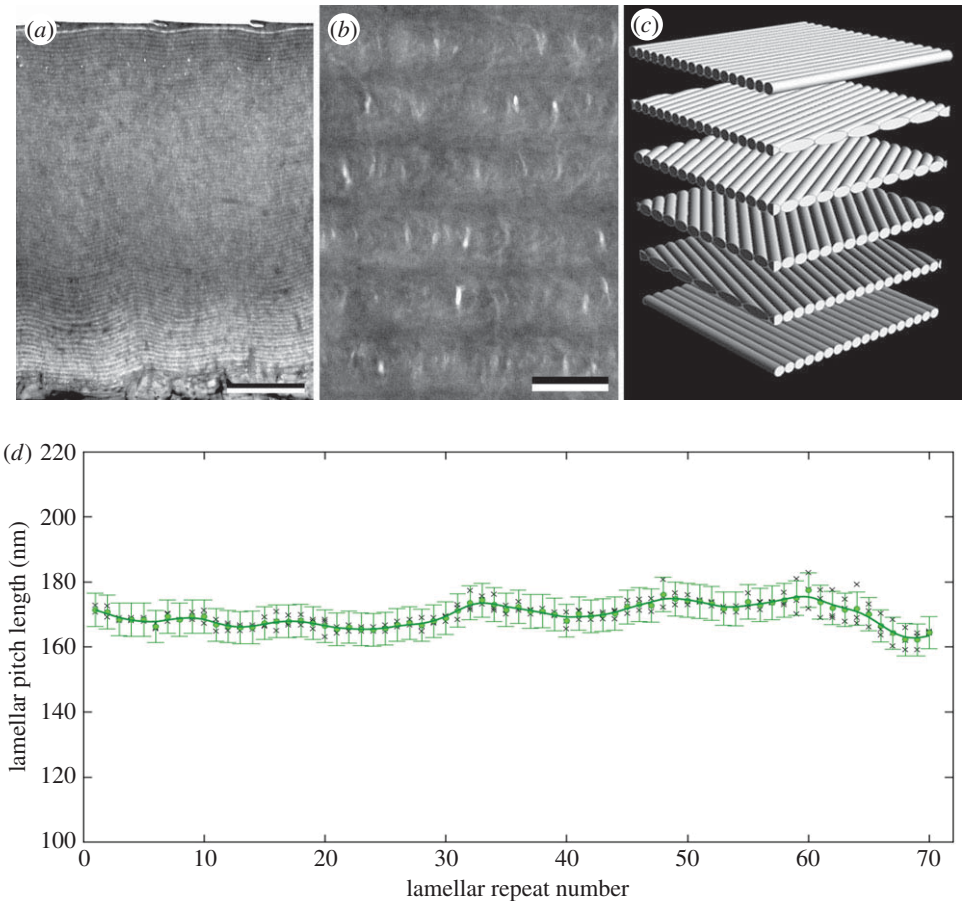

Figure 4. (*a*) TEM cross-section showing the full extent of the photonic ultrastructure within the specimen's dorsal pygidial cuticle. (*b*) High-magnification TEM cross-section showing the Bouligand structure within the beetle's elytral exocuticle. (*c*) Schematic of the helicoidal morphology within the *C. smaragdina* exocuticle. The helicoid is formed by a lamellar stack comprising successively rotated chitin microfibril layers. (*d*) Lamellar pitch profile describing the distribution of helicoidal periods in *C. smaragdina*. Each lamellar pitch measurement (black crosses) represents the distance for which the chitin microfibrils comprising the helicoid rotate through 180°. The mean lamellar pitch measurements (green circles) fitted using a spline interpolation (green line) are also shown. Scale bars, (*a*) 3 μm and (*b*) 200 nm.

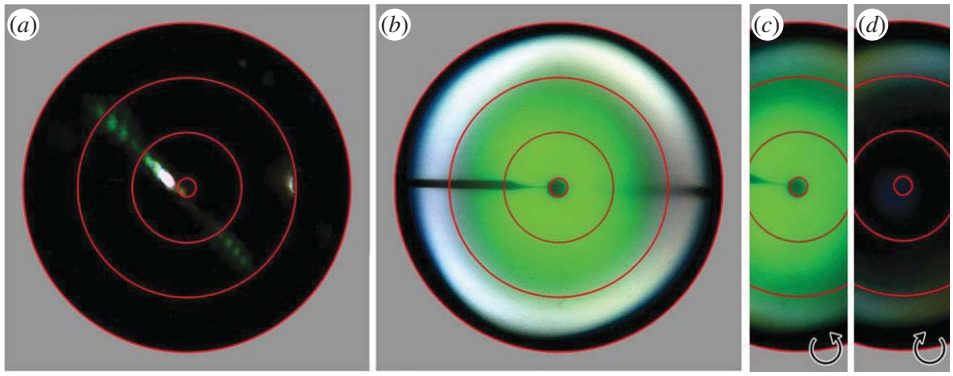

Figure 5. ISM results obtained for *C. smaragdina*, showing the far-field scattering arising following (*a*) narrow-aperture illumination and (*b*–*d*) wide-aperture illumination using the ISM. (*c*,*d*) Angle-dependent scattering pattern upon insertion of a left- and right-handed circular polarizer in the detection pathway. The images are cropped around the central axis due to polarization accuracy. Moving radially outwards from the scatterogram centres, the red circles denote scattering angles of 5°, 30°, 60° and 90°.

structures found in biological systems. The cardinal factor that determines the handedness of the reflected light is the direction of rotation in which the helicoidal ultrastructure assembles prior to sclerotization. The reflection of LCP light is manifested by an anticlockwise rotation of the helicoidal architecture. From the TEM-constructed lamellar pitch profile (figure 4*d*), we were able to establish the average pitch of the helicoid ($\approx 340 \pm 10$ nm). At normal incidence, periodic helicoidal structures exhibit Bragg reflection, with a peak wavelength, λ_0, given by $\lambda_0 = 2d\bar{n}$, where $\bar{n}$ represents the average refractive index and d is the lamellar pitch length (or helicoidal half-pitch) [21,65]. It should be noted that over many repeat measurements of the CP reflectance, small variations in the LCP spectral profile were observed in response to localized changes to the area of illumination, with the greatest variability occurring for the long-wavelength band-edge. This can be attributed to the undulations observed in the lamellar pitch distribution profile; where

more prominent peaks in the pitch occur closer to the proximal edge of the exocuticle, an increase in the longer-wavelength component of the reflection is observed.

Typically, spectral measurements of *C. smaragdina* showed peak reflectance at $\approx 560-570$ nm; a Bragg response at these wavelengths is satisfied by $\bar{n} \approx 1.647-1.676$. The existing literature provides a broad range for the refractive index of chitinous material encountered in the ultrastructure of arthropods [53,64,66–69]; here, simulations of the CP reflection observed for *C. smaragdina* were informed using Caveney's measurement of the average refractive index for the cetoniine specimen *Protaetia* (formerly *Potosia*) *speciosissima* ($\bar{n} = 1.595$) [53] and, also, wavelength-dependent refractive index data for chitin and uric acid published by Vargas *et al.* [70]. In this case, the authors performed measurements on fresh shrimp shells. Although smaller, Caveney's value is comparable to that anticipated by the spectral measurements; however, its use does lead to the modelled LCP bandgap being slightly blue-shifted. Further considering the applicability of this refractive index value, it is noted that concurrent investigations into the optical characteristics of broadband reflecting scarabaeids indicated that the cuticle incurs a small degree of shrinkage (approx. 5–10%) during the TEM preparation process. This artefact represents a historical challenge faced when preparing biological samples for TEM [71]. To facilitate a direct comparison between measured and modelled spectra, close agreement with the experimentally measured LCP spectra was achieved (figure 2) by applying a scaling factor of 1.05 to the sublayer thicknesses defining the modelled structure (figure 4*d*).

The electromagnetic simulations of the CP response further predicted a greater LCP reflectance than measured in experiments. A number of previous studies concerning the reflection of CP light by coleopteran species have focused upon rutelinid scarabs belonging to the *Chrysina* genus [20,21,72–74]. Several of these beetles display silver and gold hues owing the chirped distribution of pitch lengths within their helicoids [62,72,73,75]. Additionally, the intensity of LCP light reflected by these brilliantly coloured specimens, in response to illumination at normal incidence, exceeds that observed herein for *C. smaragdina* [72]. This result requires consideration since the number of full rotations of the *C. smaragdina* helicoid (≈ 35) is only slightly fewer than typically observed in broadband *Chrysina* specimens (≈ 40). Furthermore, the lamellar pitch lengths measured for *C. smaragdina's* narrowband reflecting cuticle are concentrated over a far narrower range of values, which should increase the reflected intensity.

Two likely factors are considered as contributing to the lower luminance measured for *C. smaragdina*. Firstly, Caveney demonstrated that the coruscating precious metal-like colours of species such as *Chrysina resplendens* are reliant on the presence of uric acid within the ultrastructure, which enhances its birefringence significantly [53]. Indeed, the birefringence in species such as *Chrysina aurigans* has been reported to be as high as 0.19 [76]. By contrast, Caveney reported an absence of uric acid in the exocuticle of *P. speciosissima*, subsequently measuring the birefringence to be 0.018 [53]. In the view of this factor, we have considered the refractive index data of both Caveney and Vargas *et al.* [70]. By applying an effective medium approximation, the effect of altering the concentration of uric acid can be explored. Following Caveney's conclusion that *P. speciosissima* contains no uric acid component, the data presented by Vargas *et al.* indicates that a structure comprised purely of chitin has an average refractive index of ≈ 1.55 at 525 nm. Of course, the hierarchical structures formed by scarab beetles and crustaceans likely exhibit differences in how they incorporate chitin crystallites into a protein matrix. Subsequently, by adopting the measurements published by Vargas *et al.* [70] we found that a uric acid fraction of 0.2 yielded Caveney's value of 1.595 at 525 nm while also accounting for material dispersion.

Consequently, the reduced specular CP reflection from *C. smaragdina* may be principally attributed to the absence, or at least low concentration, of uric acid in the structure since this limits the birefringence achievable within the exocuticle structure. We note, however, that the scattering from the surface topography will also play an important role, as is discussed in the following section.

4.2. Optical effect of the surface topography

The reticulated surface topography exhibited by *C. smaragdina* was elucidated initially through optical microscopy (figure 1) and in more detail via SEM and AFM measurements (figure 3). As illustrated in figure 5*a*, the diffractive scattering that results due to this component of the specimen's structure reflects a proportion of incident light away from the direction normal to the sample surface. As a result, the amount of incident light that interacts with the underlying helicoid is modulated.

The optical scattering behaviour resulting from the blazed grating-like surface topography encountered for *C. smaragdina* is elucidated in the imaging scatterogram shown in figure 5*a*. Diffracted orders are observed perpendicular to the direction in which the specimen's surface striations are oriented. Clear resolution of the individual diffracted modes captured in figure 5*a* is only accessible via narrow-beam illumination and requires a small beam spot. The quasi-order resulting from the imperfect geometry of the blazed architecture leads to increased interference between the elements of the diffraction pattern as the size of the illumination spot increases. Overall, the optical characteristics arising from blazed grating-like structures have received little attention in beetle species, and are more typically associated with photonic systems in Lepidoptera [77,78]. Other lepidopteran species, notably *Morpho* [79] and *Ancyluris* [80] butterflies, have also been reported to exhibit highly directional scattering. Diffraction gratings enabling spectral iridescence are by no means uncommon amongst coleopteran species, however, having been identified in one of the earliest electron microscope studies of structurally coloured insects [81]. Across several papers, Hinton & Gibbs described diffraction gratings in phalacrid [82], carabid [83] and gyrinid [84] beetles.

One report describing similar blazed grating structures in cetoniine scarabs was made by Xu *et al.* [85]. The authors examined three species of cetoniine scarab beetles, all of which possess topographical surface features remarkably similar to those observed here for *C. smaragdina*. SEM images of the specimens investigated by Xu *et al.* [85], which belong to the *Mycterophallus* and *Lomaptera* genera, revealed striations with a finer periodicity than that observed for *C. smaragdina* in two of the three specimens examined. These species exhibited a grating periodicity between 1 and 2 μm. Moreover, both these species displayed the sawtooth-like profile along the striation edges with greater regularity relative to *C. smaragdina*. The third beetle appeared to show grating dimensions closer to those of *C. smaragdina* ($\approx 4-5$ μm), although the relatively

small surface area displayed in the image limited the extent to which comparisons could be made. Qualitative analysis of the beetles appeared to show each beetle exhibiting spectral iridescence under 'bright' illumination [85].

Beyond confirming the reflection of LCP light in two of the investigated specimens, the authors offered no additional insight into the CP behaviour exhibited by the beetles. The observation of CP reflected light for species belonging to the *Lomaptera* genus has been reported elsewhere, first by Neville & Caveney [37], and, more recently, by Carter *et al.* [86], although, neither makes reference to the beetles' surface topography. Xu *et al.* [85] presented a simplified model for the origin of the reflectance of the exocuticle structures revealed via TEM cross-sections, in which traditional multilayer reflectors, formed from alternating layers comprising distinct materials of high and low refractive index, were assumed. While such reflectors are common among coleopteran species, and indeed many other one-dimensional biological photonic systems, this scalar approximation neglects the chiral aspect of the cuticle and the resulting CP component of the observed reflectance.

For wide-beam illumination, the scattering imparted by the surface topography is less obvious since the structure is being simultaneously illuminated over all incident angles. In optics, stratified structures exhibiting appropriate periodicity tend to behave as one-dimensional photonic crystals. For specularly reflecting systems, illumination at oblique angles results in iridescence manifested as a blue-shift in the reflected colour; the wavelength of the first-order Bragg reflection peak is given by $\lambda = 2d\bar{n}\cos(\theta)$, where θ is the angle between the propagation direction and the axis of the helicoid [87]. However, as indicated by the scatterograms corresponding to the unpolarized and LCP−LCP co-polarized configurations (figure 5*b*,*c*), *C. smaragdina's* blazed surface profile may suppress the iridescent response from the underlying helicoidal reflector. The ensemble colour is attributed to the sum of the scattered reflections, with additional interference attributed to the irregularities observed in the surface topography. Indeed, the beetle's green colour is expected to extend to high scattering angles as evidenced by dark-field optical microscopy observations (figure 1*e*). Similar effects, albeit from different structural configurations, have previously been observed in wide-beam illumination scatterometry of weevil scales [17] and of the dorsal wing scales of the butterfly *Parides sesostris* [88]. In the weevils' case, their elytral scales comprise many differently oriented crystal domains. The interference of reflected light from the individual domains creates an additive effect that gives rise to an angle-independent colour appearance [17]. *Parides sesostris*, on the other hand, uses an entirely different mechanism; a pigmented honeycomb structure situated in the upper lamina of the elytra inhibits the iridescent behaviour arising from its gyroid photonic crystal structure [88].

4.3. Biological significance

The question of whether this dual structural colour producing system is designed to fulfil a precise ecological function cannot be answered conclusively. Cetoniinae primarily feed from the entomophilous flowers of tropical rainforest flora and are diurnally active, therefore, the green colour appearance of *C. smaragdina* is anticipated to aid its camouflage against potential predators. Additional optical functionality may be provided by the beetle's surface topography; by acting to both reduce the intensity of the specular reflection from the beetle's surface and suppressing iridescence, the grating structure may further assist crypsis among the Indonesian rainforest. This represents a deviation from grating structures that produce spectral iridescence, which have been hypothesized to have either aposematic functionality, or to confuse depth- and/or colour-perception in predators [12].

On the other hand, as the three flower chafers investigated by Xu *et al.* were predominantly red or black in colour [85], any visual benefit may be secondary; it is equally possible that non-visual functionality may have driven the evolution of grating structures in certain Coleoptera. It has been suggested that diffraction gratings provide friction-reducing and water-repellent capabilities to certain beetles and that blazed gratings, in particular, allow burrowing species movement in compressed environments [12]. However, this behaviour is not typically associated with cetoniine species.

While Bouligand-type structures are extremely common in crustaceans, significantly enhancing the mechanical strength of their exoskeletal armours [44,45], it is not immediately obvious why this morphology would be adopted in some coleopteran species but not others unless it serves an alternative purpose. At present, the visual systems of Coleoptera represents a gap in the general breadth of knowledge concerning arthropod vision. For example, it is known that fluorescent signalling is used by birds [89], spiders [90], fish [91] and mantis shrimp [92]. More pertinently, stomatopods can detect CP stimuli [93] and, further, actively rotate their eyes to align particular photoreceptors to optimize their detection of polarized signals [94]. Some debate remains as to whether scarabaeid beetles are capable of detecting CP signals. Brady & Cummings reported that the jewel scarab *Chrysina gloriosa* is capable of differentiating between light sources of equal intensity based upon their polarization signatures alone [95]. By contrast, another jewel scarab, *C. woodi*, exhibited no phototactic discrimination. Moreover, Blaho *et al.* [96] investigated four scarab beetles including two cetoniine species, *Cetonia aurata* and *Potosia cuprea*, finding no evidence of a behavioural repsonse to CP light. Clearly, further behavioural experiments have to resolve this enigma. In addition to considering the potential biological significance of the reflecting and scattering structures encountered in these beetles, the developing understanding of their optical function also serves to inform future biomimetic technologies. For example, cellulose nano-crystals are the subject of efforts to create synthetic helicoidal architectures [97].

5. Conclusion

The flower chafer *C. smaragdina* displays a metallic green colour appearance. As described for beetles belonging to several other subfamilies of Scarabaeidae, the colour of *C. smaragdina* arises due to the helicoidal ultrastructure of its exocuticle, which performs as a Bragg reflector of LCP light, as previously described for beetles belonging to several other subfamilies of Scarabaeidae. Unlike the majority of beetles exhibiting CP reflection properties, however, *C. smaragdina* possesses a quasi-regular blazed grating surface structure. As a consequence, *C. smaragdina* exhibits the angle-independent suppression of the reflection of RCP light, while the scattering of light by the beetle's surface topography enhances the angle-independence of its green colour. In this way, the blazed surface topography may assist in modulating the metallic appearance of

C. smaragdina sufficiently that it is afforded more complete camouflage when feeding on the surface of rainforest flora.

Authors' contributions. L.T.M. performed experiments, analysed experiments, participated in the design of the study and drafted the manuscript; E.D.F. analysed experiments and drafted the manuscript; B.D.W. analysed experiments and drafted the manuscript; P.V. designed the study, coordinated the study and drafted the manuscript. All authors gave final approval for publication.

Competing interests. We declare we have no competing interests.

Funding. L.T.M., E.D.F. and P.V. acknowledge the financial support from Air Force Office of Scientific Research grant no. FA9550-10-1-0020. B.D.W. acknowledges financial support from the National Centre of Competence in Research Bio-Inspired Materials and the Ambizione programme of the Swiss National Science Foundation SNSF (168223).

Acknowledgements. The authors would also like to thank P. Splatt for assisting in preparing samples for TEM.

References

1. Thompson DW. 1961 *On growth and form*. Cambridge, UK: Cambridge University Press.
2. Turing AM. 1952 The chemical basis of morphogenesis. *Phil. Trans. R. Soc. B* **237**, 37–72. (doi:10.1098/rstb.1952.0012)
3. Douady SZ, Couder Y. 1992 Phyllotaxis as a self-organized growth process. *Phys. Rev. Lett.* **68**, 2098–2103. (doi:10.1103/PhysRevLett.68.2098)
4. Neville AC. 1993 *Biology of fibrous composites*. Cambridge, UK: Cambridge University Press.
5. Meyers MA, Chen PY, Lin AYM, Seki Y. 2008 Biological materials: structure and mechanical properties. *Prog. Mater. Sci.* **53**, 1–206. (doi:10.1016/j.pmatsci.2007.05.002)
6. Fox DL. 1976 *Animal biochromes and structural colours: physical, chemical, distributional and physiological features of coloured bodies in the animal world*. Berkeley, CA: University of California Press.
7. Srinivasarao M. 1999 Nano-optics in the biological world: beetles, butterflies, birds, and moths. *Chem. Rev.* **99**, 1935–1961. (doi:10.1021/cr970080y)
8. Vukusic P, Sambles JR. 2003 Photonic structures in biology. *Nature* **424**, 852–855. (doi:10.1038/nature01941)
9. Lee LP, Szema R. 2005 Inspirations from biological optics for advanced photonic systems. *Science* **310**, 1148–1150. (doi:10.1126/science.1115248)
10. Parker AR, Townley HE. 2007 Biomimetics of photonic nanostructures. *Nat. Nanotechnol.* **2**, 347–353. (doi:10.1038/nnano.2007.152)
11. Phan L, Kautz R, Leung EM, Naughton KL, Van Dyke Y, Gorodetsky AA. 2016 Dynamic materials inspired by cephalopods. *Chem. Mater.* **28**, 6804–6816. (doi:10.1021/acs.chemmater.6b01532)
12. Seago AE, Brady P, Vigneron JP, Schultz TD. 2009 Gold bugs and beyond: a review of iridescence and structural colour mechanisms in beetles (Coleoptera). *J. R. Soc. Interface* **6**, S165–S184. (doi:10.1098/rsif.2008.0354.focus)
13. Parker AR, McKenzie DR, Large MCJ. 1998 Multilayer reflectors in animals using green and gold beetles as contrasting examples. *J. Exp. Biol.* **201**, 1307–1313.
14. Lenau T, Barfoed M. 2008 Colours and metallic sheen in beetle shells — a biomimetic search for material structuring principles causing light interference. *Adv. Eng. Mater.* **10**, 299–314. (doi:10.1002/adem.200700346)
15. Schultz TD, Bernard GD. 1989 Pointillistic mixing of interference colours in cryptic tiger beetles. *Nature* **337**, 72–73. (doi:10.1038/337072a0)
16. Pouya C, Stavenga DG, Vukusic P. 2011 Discovery of ordered and quasi-ordered photonic crystal structures in the scales of the beetle *Eupholus magnificus*. *Opt. Express* **19**, 11 355–11 364. (doi:10.1364/OE.19.011355)
17. Wilts BD, Michielsen K, Kuipers J, De Raedt H, Stavenga DG. 2012 Brilliant camouflage: photonic crystals in the diamond weevil, *Entimus imperialis*. *Proc. R. Soc. B* **279**, 2524–2530. (doi:10.1098/rspb.2011.2651)
18. Vukusic P, Hallam B, Noyes J. 2007 Brilliant whiteness in ultrathin beetle scales. *Science* **315**, 348. (doi:10.1126/science.1134666)
19. Burresi M, Cortese L, Pattelli L, Kolle M, Vukusic P, Wiersma DS, Steiner U, Vignolini S. 2014 Bright-white beetle scales optimise multiple scattering of light. *Sci. Rep.* **4**, 6075. (doi:10.1038/srep06075)
20. Jewell SA, Vukusic P, Roberts NW. 2007 Circularly polarized colour reflection from helicoidal structures in the beetle *Plusiotis boucardi*. *New J. Phys.* **9**, 99. (doi:10.1088/1367-2630/9/4/099)
21. Sharma V, Crne M, Park JO, Srinivasarao M. 2009 Structural origin of circularly polarized iridescence in jeweled beetles. *Science* **325**, 449–451. (doi:10.1126/science.1172051)
22. Arwin H, Magnusson R, Landin J. 2012 Chirality-induced polarization effects in the cuticle of scarab beetles: 100 years after Michelson. *Philos. Mag.* **92**, 1583–1599. (doi:10.1080/14786435.2011.648228)
23. Shashar N, Hanlon RT, Petz A. 1998 Polarization vision helps detect transparent prey. *Nature* **393**, 222–223. (doi:10.1038/30380)
24. Shashar N, Hagan R, Boal JG, Hanlon RT. 2000 Cuttlefish use polarization sensitivity in predation on silvery fish. *Vision Res.* **40**, 71–75. (doi:10.1016/S0042-6989(99)00158-3)
25. von Frisch K. 1949 Die Polarisation des Himmelslichtes als orientierender Faktor bei den Tänzen der Bienen. *Experientia* **5**, 142–148. (doi:10.1007/BF02174424)
26. Wehner R. 1976 Polarized-light navigation by insects. *Sci. Am.* **235**, 106–115. (doi:10.1038/scientificamerican0776-106)
27. Sweeney A, Jiggins C, Johnsen S. 2003 Polarized light as a butterfly mating signal. *Nature* **423**, 31–32. (doi:10.1038/423031a)
28. Gagnon YL, Templin RM, How MJ, Justin Marshall N. 2015 Circularly polarized light as a communication signal in mantis shrimps. *Curr. Biol.* **25**, 3074–3078. (doi:10.1016/j.cub.2015.10.047)
29. Vukusic P, Sambles JR, Lawrence CR. 2000 Colour mixing in wing scales of a butterfly. *Nature* **404**, 457. (doi:10.1038/35006561)
30. Hooper IR, Vukusic P, Wootton RJ. 2006 Detailed optical study of the transparent wing membranes of the dragonfly *Aeshna cyanea*. *Opt. Express* **14**, 4891–4897. (doi:10.1364/OE.14.004891)
31. Yoshioka S, Kinoshita S. 2007 Polarization-sensitive color mixing in the wing of the Madagascan sunset moth. *Opt. Express* **15**, 2691–2701. (doi:10.1364/OE.15.002691)
32. Stavenga DG, Wilts BD, Leertouwer HL, Hariyama T. 2011 Polarized iridescence of the multilayered elytra of the Japanese jewel beetle, *Chrysochroa fulgidissima*. *Phil. Trans. R. Soc. B* **366**, 709–723. (doi:10.1098/rstb.2010.0197)
33. Michelson AA. 1911 On metallic colouring in birds and insects. *Philos. Mag.* **21**, 554–567. (doi:10.1080/14786440408637061)
34. Gaubert P. 1924 Sur la polarisation circulaire de la lumière réfléchie par les insectes. *Comptes rendus* **179**, 1148–1150.
35. Mathieu JP, Faraggi N. 1937 Étude de la lumière polarisée circulairements réfléchie par certains coléoptères. *Comptes rendus* **205**, 1378–1380.
36. Robinson C. 1966 The cholesteric phase in polypeptide solutions and biological structures. *Mol. Cryst.* **1**, 467–494. (doi:10.1080/15421406608083287)
37. Neville AC, Caveney S. 1969 Scarabaeid beetle exocuticle as an optical analogue of cholesteric liquid crystals. *Biol. Rev.* **44**, 531–562. (doi:10.1111/j.1469-185X.1969.tb00611.x)
38. Bouligand Y. 1972 Twisted fibrous arrangements in biological materials and cholesteric mesophases. *Tissue Cell* **4**, 189–217. (doi:10.1016/S0040-8166(72)80042-9)
39. Pace A. 1972 Cholesteric liquid crystal-like structure of the cuticle of *Plusiotis gloriosa*. *Science* **176**, 678–680. (doi:10.1126/science.176.4035.678)
40. Neville A, Luke B. 1969 A two-system model for chitin–protein complexes in insect cuticles. *Tissue Cell* **1**, 689–707. (doi:10.1016/S0040-8166(69)80041-8)
41. Wilts BD, Whitney HM, Glover BJ, Steiner U, Vignolini S. 2014 Natural helicoidal structures: morphology, self-assembly and optical properties.

Mater. Today Proc. **1**, 177–185. (doi:10.1016/j.matpr.2014.09.021)
42. Gubb D. 1975 A direct visualisation of helicoidal architecture in *Carcinus maenas* and *Halocynthia papillosa* by scanning electron microscopy. *Tissue Cell* **7**, 19–32. (doi:10.1016/S0040-8166(75)80005-X)
43. Giraud-Guille MM. 1984 Fine structure of the chitin–protein system in the crab cuticle. *Tissue Cell* **16**, 75–92. (doi:10.1016/0040-8166(84)90020-X)
44. Raabe D, Sachs C, Romano P. 2005 The crustacean exoskeleton as an example of a structurally and mechanically graded biological nanocomposite material. *Acta Mater.* **53**, 4281–4292. (doi:10.1016/j.actamat.2005.05.027)
45. Weaver JC *et al.* 2012 The stomatopod dactyl club: a formidable damage-tolerant biological hammer. *Science* **336**, 1275–1280. (doi:10.1126/science.1218764)
46. Grunenfelder LK *et al.* 2014 Bio-inspired impact-resistant composites. *Acta Biomater.* **10**, 3997–4008. (doi:10.1016/j.actbio.2014.03.022)
47. Vignolini S, Rudall PJ, Rowland AV, Reed A, Moyroud E, Faden RB, Baumberg JJ, Glover BJ, Steiner U. 2012 Pointillist structural color in *Pollia* fruit. *Proc. Natl Acad. Sci. USA* **109**, 15 712–15 715. (doi:10.1073/pnas.1210105109)
48. Vignolini S, Gregory T, Kolle M, Lethbridge A, Moyroud E, Steiner U, Glover BJ, Vukusic P, Rudall PJ. 2016 Structural colour from helicoidal cell-wall architecture in fruits of *Margaritaria nobilis*. *J. R. Soc. Interface* **13**, 20160645. (doi:10.1098/rsif.2016.0645)
49. Neville AC, Levy S. 1984 Helicoidal orientation of cellulose microfibrils in *Nitella opaca* internode cells: ultrastructure and computed theoretical effects of strain reorientation during wall growth. *Planta* **162**, 370–384. (doi:10.1007/BF00396750)
50. Gould KS, Lee DW. 1996 Physical and ultrastructural basis of blue leaf iridescence in four Malaysian understory plants. *Am. J. Bot.* **83**, 45–50. (doi:10.2307/2445952)
51. Goldstein DH. 2006 Polarization properties of Scarabaeidae. *Appl. Opt.* **45**, 7944–7950. (doi:10.1364/AO.45.007944)
52. Pye JD. 2010 The distribution of circularly polarized light reflection in the Scarabaeoidea (Coleoptera). *Biol. J. Linn. Soc.* **100**, 585–596. (doi:10.1111/j.1095-8312.2010.01449.x)
53. Caveney S. 1971 Cuticle reflectivity and optical activity in scarab beetles: the role of uric acid. *Proc. R. Soc. Lond. B* **178**, 205–225. (doi:10.1098/rspb.1971.0062)
54. Hodgkinson I, Lowrey S, Bourke L, Parker A, McCall MW. 2010 Mueller-matrix characterization of beetle cuticle: polarized and unpolarized reflections from representative architectures. *Appl. Opt.* **49**, 4558–4567. (doi:10.1364/AO.49.004558)
55. Stavenga DG, Leertouwer HL, Pirih P, Wehling MF. 2009 Imaging scatterometry of butterfly wing scales. *Opt. Express* **17**, 193–202. (doi:10.1364/OE.17.000193)
56. Wilts BD, Michielsen K, De Raedt H, Stavenga DG. 2012 Hemispherical Brillouin zone imaging of a diamond-type biological photonic crystal. *J. R. Soc. Interface* **9**, 1609–1614. (doi:10.1098/rsif.2011.0730)
57. Berreman DW. 1972 Optics in stratified and anisotropic media: 4 × 4-matrix formulation. *J. Opt. Soc. Am.* **62**, 502–510. (doi:10.1364/JOSA.62.000502)
58. Yeh P. 1979 Electromagnetic propagation in birefringent layered media. *J. Opt. Soc. Am.* **69**, 742–756. (doi:10.1364/JOSA.69.000742)
59. Lin-Chung PJ, Teitler S. 1984 4 × 4 Matrix formalisms for optics in stratified anisotropic media. *J. Opt. Soc. Am. A* **1**, 703–705. (doi:10.1364/JOSAA.1.000703)
60. Ko DYK, Sambles JR. 1988 Scattering matrix method for propagation of radiation in stratified media: attenuated total reflection studies of liquid crystals. *J. Opt. Soc. Am.* **5**, 1863–1866. (doi:10.1364/JOSAA.5.001863)
61. Gory H, Percheron A. 1833 *Monographie des Cétoines et genres voisins, formant, dans les familles naturelles de Latreille, la division des Scarabées mélitophiles*. Paris: J.-B. Baillière.
62. Neville AC. 1977 Metallic gold and silver colours in some insect cuticles. *J. Insect Physiol.* **23**, 1267–1274. (doi:10.1016/0022-1910(77)90069-5)
63. Hariyama T, Hironaka M, Horiguchi H, Stavenga DG. 2005 The leaf beetle, the jewel beetle, and the damselfly; insects with a multilayered show case. In *Structural colors in biological systems: principles and applications* (eds S Kinoshita, S Yoshioka), pp. 153–176. Osaka University Press.
64. Noyes JA, Vukusic P, Hooper IR. 2007 Experimental method for reliably establishing the refractive index of buprestid beetle exocuticle. *Opt. Express* **15**, 4351–4358. (doi:10.1364/OE.15.004351)
65. de Vries H. 1951 Rotatory power and other optical properties of certain liquid crystals. *Acta Crystallogr.* **4**, 219–226. (doi:10.1107/S0365110X51000751)
66. Brink DJ, Lee ME. 1996 Ellipsometry of diffractive insect reflectors. *Appl. Opt.* **35**, 1950–1955. (doi:10.1364/AO.35.001950)
67. Brink DJ, Lee ME. 1998 Thin-film biological reflectors: optical characterization of the *Chrysiridia croesus* moth. *Appl. Opt.* **37**, 4213–4217. (doi:10.1364/AO.37.004213)
68. Leertouwer HL, Wilts BD, Stavenga DG. 2011 Refractive index and dispersion of butterfly chitin and bird keratin measured by polarizing interference microscopy. *Opt. Express* **19**, 24 061–24 066. (doi:10.1364/OE.19.024061)
69. Yoshioka S, Kinoshita S. 2011 Direct determination of the refractive index of natural multilayer systems. *Phys. Rev. E* **83**, 051917. (doi:10.1103/PhysRevE.83.051917)
70. Vargas WE, Azofeifa DE, Arguedas HJ. 2013 Refractive indices of chitin, chitosan, and uric acid with application to structural color analysis. *Opt. Pura y Apl.* **46**, 55–72. (doi:10.7149/OPA.46.1.55)
71. Crang RFE, Klomparens KL (eds). 1988 *Artifacts in biological electron microscopy*. New York, NY: Plenum Press.
72. McDonald L, Finlayson E, Vukusic P. 2015 Untwisting the polarization properties of light reflected by scarab beetles. *Prog. Biomed. Opt. Imaging - Proc. SPIE* **9341**. (doi:10.1117/12.2079496)
73. Vargas WE, Hernández-Jiménez M, Libby E, Azofeifa DE, Barboza C, Solís Á. 2016 Light reflection by cuticles of *Chrysina* jewel scarabs: optical measurements, morphology characterization, and theoretical modeling. *Opt. Photonics J.* **6**, 146–163. (doi:10.4236/opj.2016.67017)
74. Fernández del Río L, Arwin H, Järrendahl K. 2016 Polarizing properties and structure of the cuticle of scarab beetles from the *Chrysina* genus. *Phys. Rev. E* **94**, 012409. (doi:10.1103/PhysRevE.94.012409)
75. Cook CQ, Amir A. 2016 Theory of chirped photonic crystals in biological broadband reflectors. *Optica* **3**, 1436–1439. (doi:10.1364/OPTICA.3.001436)
76. Azofeifa D, Hernández-Jiménez M, Libby E, Solís Á, Barboza-Aguilar C, Vargas W. 2015 A quantitative assessment approach of feasible optical mechanisms contributing to structural color of golden-like *Chrysina aurigans* scarab beetles. *J. Quant. Spectrosc. Radiat. Transf.* **160**, 63–74. (doi:10.1016/j.jqsrt.2015.03.014)
77. Ingram AL, Lousse V, Parker AR, Vigneron JP. 2008 Dual gratings interspersed on a single butterfly scale. *J. R. Soc. Interface* **5**, 1387–1390. (doi:10.1098/rsif.2008.0227)
78. Vigneron JP, Kertész K, Vértesy Z, Rassart M, Lousse V, Bálint Z, Biró LP. 2008 Correlated diffraction and fluorescence in the backscattering iridescence of the male butterfly *Troides magellanus* (Papilionidae). *Phys. Rev. E* **78**, 021903. (doi:10.1103/PhysRevE.78.021903)
79. Vukusic P, Sambles JR, Lawrence CR, Wootton RJ. 1999 Quantified interference and diffraction in single *Morpho* butterfly scales. *Proc. R. Soc. Lond. B* **266**, 1403–1411. (doi:10.1098/rspb.1999.0794)
80. Vukusic P, Sambles JR, Lawrence CR, Wooton RJ. 2001 Now you see it — now you don't. *Nature* **410**, 36. (doi:10.1038/35065161)
81. Anderson TF, Richards AG. 1942 An electron microscope study of some structural colors of insects. *J. Appl. Phys.* **13**, 748–758. (doi:10.1063/1.1714827)
82. Hinton HE, Gibbs DF. 1969 Diffraction gratings in phalacrid beetles. *Nature* **221**, 953–954. (doi:10.1038/221953a0)
83. Hinton HE, Gibbs DF. 1969 An electron microscope study of the gratings of some carabid beetles. *J. Insect Physiol.* **15**, 959–962. (doi:10.1016/0022-1910(69)90136-X)
84. Hinton HE, Gibbs DF. 1971 Diffraction gratings in gyrinid beetles. *J. Insect Physiol.* **17**, 1023–1035. (doi:10.1016/0022-1910(71)90006-0)
85. Xu M, Seago AE, Sutherland TD, Weisman S. 2010 Dual structural color mechanisms in a scarab beetle. *J. Morphol.* **271**, 1300–1305. (doi:10.1002/jmor.10870)
86. Carter IE, Weir K, Mccall MW, Parker AR. 2016 Variation in the circularly polarised light reflection of *Lomaptera* (Scarabaeidae) beetles. *J. R. Soc. Interface* **13**, 20160015. (doi:10.1098/rsif.2016.0015)
87. Mitov M, Dessaud N. 2006 Going beyond the reflectance limit of cholesteric liquid crystals. *Nat. Mater.* **5**, 361–364. (doi:10.1038/nmat1619)

88. Wilts BD, Michielsen K, De Raedt H, Stavenga DG. 2011 Iridescence and spectral filtering of the gyroid-type photonic crystals in *Parides sesostris* wing scales. *Interface Focus* **2**, 681–687. (doi:10.1098/rsfs.2011.0082)
89. Arnold KE, Owens IPF, Marshall NJ. 2002 Fluorescent signaling in parrots. *Science* **295**, 92. (doi:10.1126/science.295.5552.92)
90. Lim MLM, Land MF, Li D. 2007 Sex-specific UV and fluorescence signals in jumping spiders. *Science* **315**, 481. (doi:10.1126/science.1134254)
91. Siebeck UE. 2004 Communication in coral reef fish: the role of ultraviolet colour patterns in damselfish territorial behaviour. *Anim. Behav.* **68**, 273–282. (doi:10.1016/j.anbehav.2003.11.010)
92. Mazel CH, Cronin TW, Caldwell RL, Marshall NJ. 2004 Fluorescent enhancement of signaling in a mantis shrimp. *Science* **303**, 51. (doi:10.1126/science.1089803)
93. Chiou TH, Kleinlogel S, Cronin T, Caldwell R, Loeffler B, Siddiqi A, Goldizen A, Marshall J. 2008 Circular polarization vision in a stomatopod crustacean. *Curr. Biol.* **18**, 429–434. (doi:10.1016/j.cub.2008.02.066)
94. Daly IM, How MJ, Partridge JC, Temple SE, Marshall NJ, Cronin TW, Roberts NW. 2016 Dynamic polarization vision in mantis shrimps. *Nat. Commun.* **7**, 12140. (doi:10.1038/ncomms12140)
95. Brady P, Cummings M. 2010 Differential response to circularly polarized light by the jewel scarab beetle *Chrysina gloriosa*. *Am. Nat.* **175**, 614–620. (doi:10.1086/651593)
96. Blahó M, Egri A, Hegedüs R, Jósvai J, Tóth M, Kertész K, Biró LP, Kriska G, Horváth G. 2012 No evidence for behavioral responses to circularly polarized light in four scarab beetle species with circularly polarizing exocuticle. *Physiol. Behav.* **105**, 1067–1075. (doi:10.1016/j.physbeh.2011.11.020)
97. Dumanli AG, Kamita G, Landman J, van der Kooij H, Glover BJ, Baumberg JJ, Steiner U, Vignolini S. 2014 Controlled, bio-inspired self-assembly of cellulose-based chiral reflectors. *Adv. Opt. Mater.* **2**, 646–650. (doi:10.1002/adom.201400112)